ABSTRACT

THE ELECTRICAL CONDUCTIVITY OF SINGLE CRYSTAL Cr_2O_3

by Julian Anthony Crawford

The electrical conductivity of single crystals of Cr_2O_3 has been measured as a function of temperature over a range of 569 to 1416°C and as a function of oxygen partial pressure over a range of 1 to 10^{-6} atm. The results show a high-temperature "intrinsic" conductivity that is independent of oxygen pressure, and a low-temperature defect-controlled conductivity that varies with oxygen pressure in a manner which cannot be determined from measurements on single crystals. The very low mobility deduced from the intrinsic conductivity leads to an interpretation in terms of the theory of small polarons. The model suggested is that of charge formation and transport in the localized 3d levels of the Cr^{3+} cations.

THE ELECTRICAL CONDUCTIVITY OF SINGLE CRYSTAL Cr_2O_3

By

Julian Anthony Crawford

A THESIS

Submitted to
Michigan State University
in partial fulfillment of the requirements
for the degree of

DOCTOR OF PHILOSOPHY

Department of Physics and Astronomy

1963

ACKNOWLEDGMENTS

I wish to express my appreciation to Dr. Robert W. Vest for his suggestion of this problem and for his guidance and encouragement throughout the work. I would also like to thank Dr. Norman M. Tallan for many stimulating discussions of the problem and its interpretation. I wish to thank Professor Donald J. Montgomery for his help and advice during the preparation of this thesis and Professor Sherwood K. Haynes for his cooperation and encouragement during my studies. The experimental research reported here was performed in the facilities of the Metallurgy and Ceramics Laboratory of the Aerospace Research Laboratories of the Office of Aerospace Research, United States Air Force.

TABLE OF CONTENTS

LIST OF TABLES

LIST OF FIGURES

I. INTRODUCTION

There has been increasing interest recently in the electrical transport properties of inorganic compounds which are insulators when very pure and stoichiometric but are quite good conductors when impure or non-stoichiometric. In particular the transition-metal oxides have received considerable attention owing to the variable-valence property of the cations. Verwey[1] has suggested for these materials the mechanism of "controlled valency," which refers to the change in valence of a small fraction of the cations brought about by the introduction of a small amount of aliovalent impurity. Heikes and Johnston[2] and van Houten[3] have used this technique to study the properties of lithium-substituted transition-metal oxides. Their findings indicate that the electrical transport in these materials can be explained by assuming that the charge carriers are localized on the cations and that conduction occurs via a thermally-activated diffusion (or hopping) process. This mechanism is characterized by rather low values of electrical conductivity and by a low carrier mobility that increases exponentially with increasing temperature. The activation energy associated with the mobility is a consequence of the self-trapping of the charge carrier by its own polarization field.

Morin[4], in an earlier approach, had analyzed data on α Fe_2O_3 and NiO in terms of the usual semiconductor band theory, and had found that the mobility of the charge carriers varied between 10^{-5} and 10^{-1} $cm^2/volt\text{-}sec$. He interpreted this mobility as being due to

conduction either in a very narrow d-band or in localized d-levels. He subsequently made a survey[5] of the magnetic, electrical, and optical properties of the 3d metal oxides in an effort to detect evidence of energy bands in these compounds. His conclusion that the non-bonding 3d electrons in the oxides of scandium, titanium, and vanadium overlap sufficiently to form a 3d conduction band was verified experimentally[6] for the lower oxides of titanium and vanadium, which show a metal-to-insulator transition at the Néel temperature. He further concluded that the 3d electrons do not overlap in the remaining 3d metal oxides, but that they are in isolated energy states; hence electrical transport occurs by electron exchange between cation neighbors and involves an activation energy.

Attempts to derive this type of activated transport mechanism from first principles have resulted in the theory of polarons. The term "polaron" is used to describe a quasi-particle consisting of an electron surrounded by an accompanying cloud of lattice polarization and moving as an entity through the lattice either by tunneling (polaron band) or by phonon-activated jumps (hopping process). The lattice polarization surrounding the electron arises from the strong electron-lattice interaction characteristic of ionic materials. Because of this strong coupling effect, the usual band theory does not apply.

There are two different theoretical approaches to this problem in the literature. The first[7] is an extension of the usual effective-mass

approximation starting with Bloch functions and utilizing a variational technique to find the energies of low-lying polaron states. This method, however, applies only for weak coupling and low temperatures. The second method, which yields results applicable to metal oxides at high temperatures, is frequently referred to as "small polaron theory". The theory as developed by Yamashita and Kurosawa[8], Sewell[9], and Holstein[10] takes the Heitler-London or tight-binding approximation as a starting point, with the electron localized on one lattice site and the centers of the lattice vibration harmonic oscillators suitably displaced by an amount depending on the strength of the electron-lattice coupling. In this theory the relative roles of the periodic potential and the electron-phonon interaction are reversed; the electron-phonon interaction is considered in zero order (to produce self-trapping), and the periodic lattice potential is treated as a perturbation which gives rise to a wandering of the polaron through the lattice. The eigenstates of the system are constructed as linear combinations of localized states. At low temperatures a polaron band is formed, which narrows as the temperature increases. At a transition temperature of the order of half the optical-phonon temperature, the polaron band width becomes comparable with the breadth of a localized state and the band picture breaks down. Above the transition temperature the electron apparently hops from site to site with an activation energy. Apart from impurity scattering, as the temperature is increased the mobility decreases at

low temperatures when the band model applies, but increases exponentially with an activation energy above the transition temperature.

Most of the theoretical work done on small polarons applies only to the pure, perfectly periodic lattice. On the other hand, most of the experimental evidence for hopping transport in the transition metal oxides has come from impure, doped samples at temperatures where the conductivity is defect controlled. Perhaps important also is the fact that most of the data were taken on polycrystalline samples for which interpretation may be somewhat doubtful. In the light of these observations it would be useful to have some more precise data from single-crystal samples taken under well-defined experimental conditions in the temperature region covered by the theoretical assumptions.

The transition metal oxide chosen for this study was chromium sesquioxide, Cr_2O_3. One of the primary factors in its choice was the availability of single crystals. Moreover, a search of the literature revealed only a scanty amount of conflicting data on the electrical conductivity at high temperatures. Hauffe and Block[11] measured the electrical conductivity of a sintered sample of pure Cr_2O_3 from 400 to 800°C by a two-terminal dc method. They observed an oxygen-pressure dependence too small to be explained by the usual defect theories. This observation led them to postulate the existence of a conductivity mechanism in chromia which is independent of oxygen pressure. Fischer and Lorenz[12] extended these measurements to 1750°C with

samples doped with Cu_2O and TiO_2, and concluded that there was no oxygen-pressure dependence from 600 to 1750°C. They observed a break in the curve at 1250°C and calculated an activation energy of 2.5 ev for the high-temperature part. More recently Hagel and Seybolt[13] used a four-terminal dc method to measure the conductivity of sintered chromia samples in air, argon, and nitrogen. They calculated a high-temperature slope of 1.7 ev and a low-temperature slope of 0.36 ev. Their data showed a very slight pressure dependence below 1250°C.

Measurement of the electrical conductivity of single-crystal samples of Cr_2O_3 in the temperature range from 600 to 1400°C should provide the answers to some of the questions raised by previous work. Controlled variation of the oxygen pressure around the sample, and the use of oriented single crystals should lead to better-defined data which will aid in interpretation of the results in terms of the available theories.

II. EXPERIMENTAL PROCEDURE

A. Sample Preparation

Single-crystal samples of pure Cr_2O_3 were obtained from Linde Company[14] in the form of cylindrical rods approximately 2 cm long and 1/2 cm in diameter. The crystals were grown by the flame-fusion method from powder of unspecified purity, but presumably of laboratory grade. Spectrochemical analyses on crystalline fragments of the boules were performed by Battelle Memorial Institute, Columbus, Ohio. The results are shown in Table I.

Table I - Atomic percent of metal impurities in Cr_2O_3 single crystal samples.

Metal Impurity	Unoriented Samples	Oriented Samples
Fe	<0.001(N)	0.003
Al	0.1	0.02
Cu	<0.001(N)	< 0.001(N)
Si	0.002	0.003
Mg	<0.001(T)	0.003
Ca	0.002	0.007
Na	<0.001(T)	< 0.001(N)
V	<0.005(N)	0.02

(N) Not detected.
(T) Trace.

Samples for measurement of electrical conductivity were cut in the form of thin plates with the appropriate geometry for parallel-plate capacitance measurements. Two samples were cut directly from a boule with no attempt at orientation. One boule was oriented by x-ray diffraction methods and two samples were cut from it, one with faces

perpendicular to the c-axis and one with faces parallel to it. Figure 1 shows a back-reflection Laue diffraction pattern for each of the oriented samples.

The samples were cut from the boules with a diamond saw, and the cut faces were polished on 240-grit wet-or-dry metallographic paper. The samples were cleaned thoroughly in acetone, given a final rinse in ether, and fired in air to approximately 800°C in a muffle furnace. The samples were then electroded by painting a thin layer of Engelhard #6082 platinum paste[15] on the polished faces. One face was coated with a single continuous film, and the opposite face was given a smaller circular inner electrode surrounded by a guard-ring electrode. The paste was fired slowly in air to approximately 450°C to remove the organic vehicle, and then heated to 800°C to fire the platinum binder. The electrode films prepared in this way had a resistance of less than one ohm.

B. Experimental Apparatus

An overall view of the experimental apparatus for the measurement of electrical conductivity is shown in Figure2. Two furnaces were built to operate with a single vacuum system so that two experiments could progress simultaneously.

A drawing of the sample holder is shown in Figure 3. The portion in the furnace is constructed entirely of recrystallized alumina (McDanel AP35 and Morganite Triangle RR) and platinum-rhodium alloys.

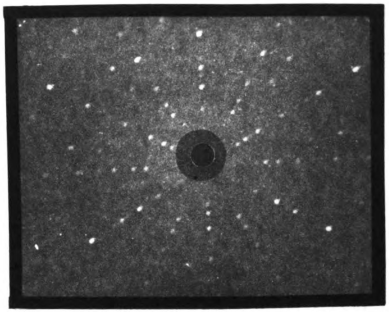

"C" - Sample

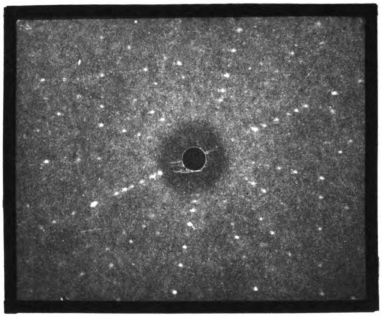

"A" - Sample

Fig. 1 - Laue photographs of oriented samples

Fig. 2 - Experimental apparatus

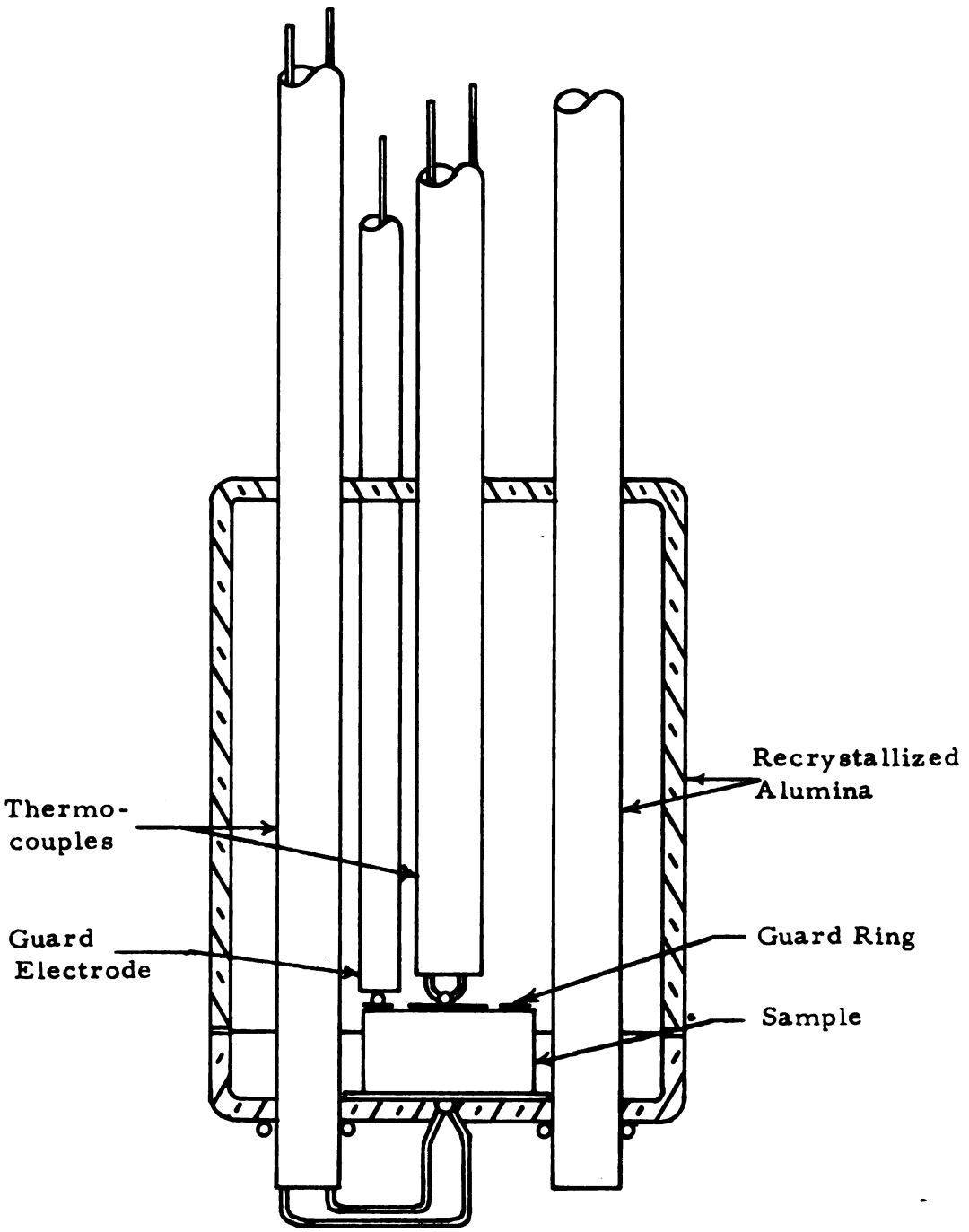

Fig. 3 - Sample holder

The sample area is enclosed by a platinum-coated crucible. The bottom of the sample holder is supported from three alumina rods, one of which carries the lower thermocouple leads. The upper thermocouple is contained in another alumina rod which is spring loaded at its upper end and is situated in the center of the assembly. The guard lead was made from platinum wire and contained in a small alumina rod, also spring loaded at the top. The two spring-loaded electrodes served to hold the sample in place against the lower electrode.

The sample holder and three radiation shields were suspended from a large brass plate which constituted the top plate of the high-temperature furnace. Figure 4 is a schematic of the furnace assembly with the sample holder in place. The furnace tube which separates the sample chamber from the furnace is McDanel AP35 recrystallized alumina which is vacuum tight up to 1800°C. The tube is cooled at each end by large water-jacketed copper collets, and is made vacuum tight by O-ring seals. The furnace element is made of tungsten wire wound on an alumina core with molybdenum and tantalum radiation shields. Power is supplied from a 0-140v, 25a variable autotransformer. The furnace power is regulated by a Minneapolis-Honeywell R 7086A Potentiometer Controller modified to achieve a sensitivity of approximately 5 microvolts. The controller responds to a platinum + 6% rhodium vs. platinum + 30% rhodium thermocouple located next to the furnace core. The temperature at the sample is held constant to within 0.5C° above 1000°C.

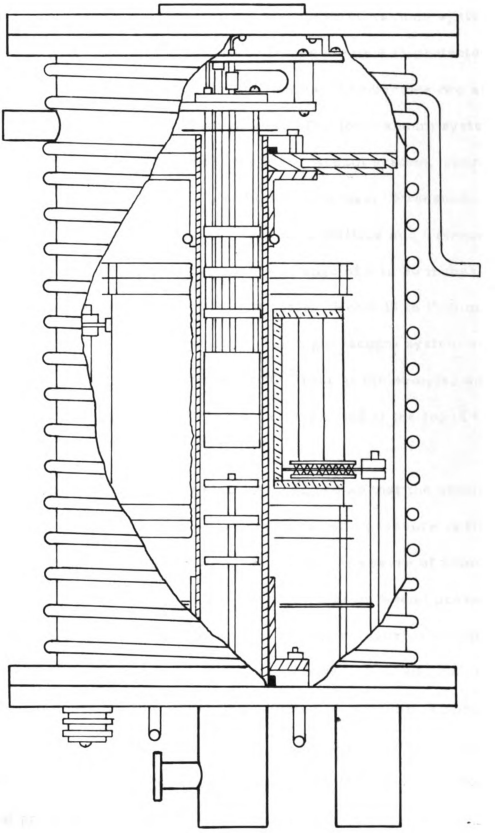

Fig. 4 - High temperature furnace and sample holder

Figure 5 is a schematic diagram of the three vacuum systems built into the apparatus. The tungsten furnace element is protected by a vacuum of better than 10^{-5} torr. The sample chamber has two separate vacuum systems to cover different ranges. The low-vacuum system, which serves as a roughing line for the high-vacuum system, operates with a mechanical pump down to less than 10 microns. Pressures from one atmosphere to 1000 microns are read on a Wallace and Tiernan Precision Dial Manometer FA 145 having a range of 0 to 30 inches of mercury and an accuracy of 0.1% of full scale. From 10 to 1000 microns a Veeco Thermocouple gauge is used. The high-vacuum system will produce a vacuum of approximately 5×10^{-5} torr at the sample, as determined by a Veeco type-RG 75 ion gauge located at the top of the furnace.

The high-temperature furnace is designed so that the atmosphere surrounding the sample can be maintained at a total pressure of from one to 10^{-6} atmosphere, and at an oxygen partial pressure of from one to approximately 10^{-20} atmosphere. Various oxygen partial pressures may be obtained by (1) blending helium-plus-water-vapor with hydrogen, (2) blending carbon dioxide with carbon monoxide, (3) mixing helium with oxygen, or (4) reducing the total oxygen pressure over the sample. In the present investigation only the latter two methods were used to vary the oxygen pressure around the sample and thereby establish the region of pressure dependence.

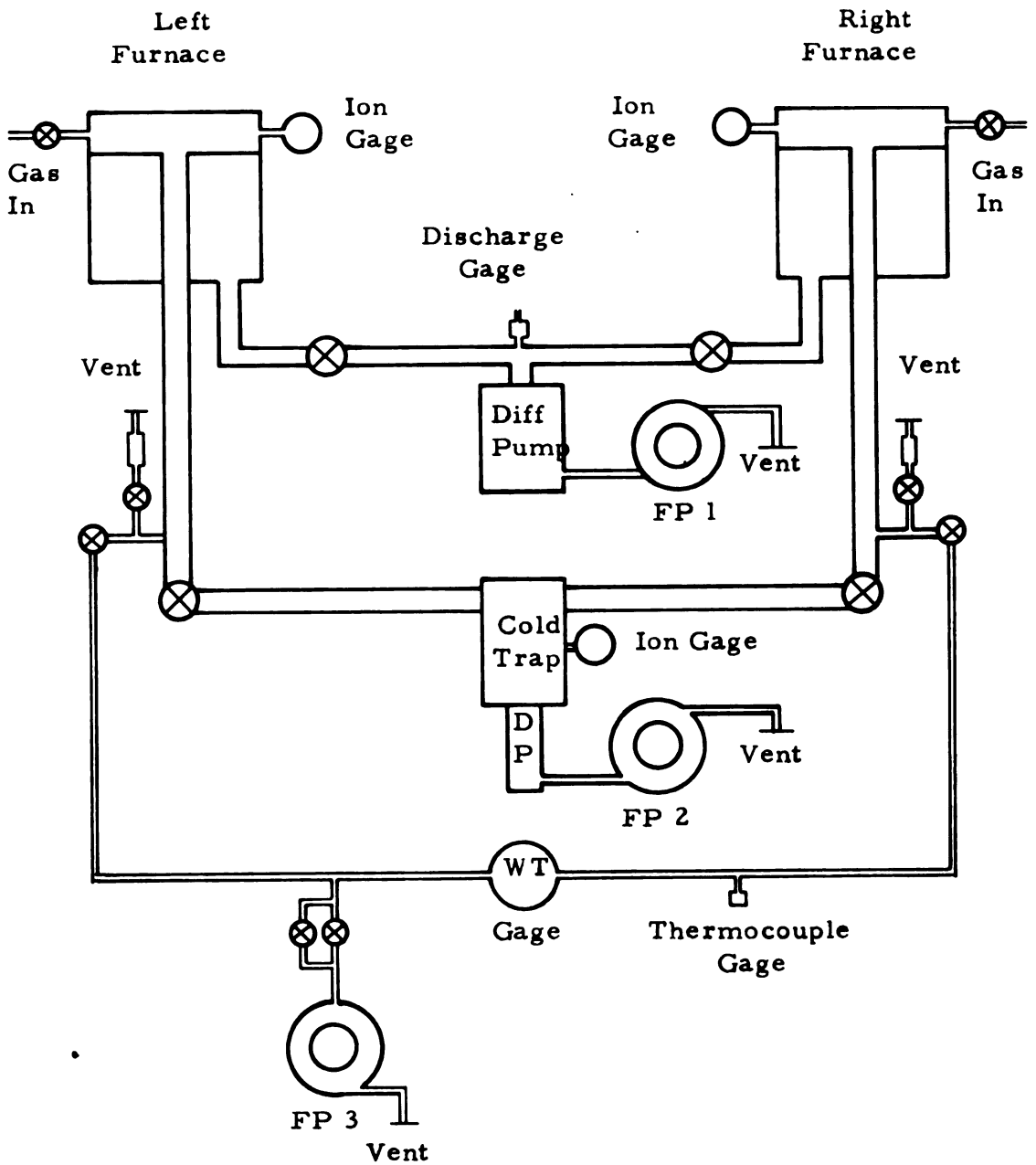

Fig. 5 - Vacuum systems

Electrical-conductivity measurements were made using both ac and dc methods in different but overlapping ranges. In the low-conductivity region, ac measurements were made on a transformer ratio-arm bridge (Wayne Kerr Universal Bridge B221) with a conductance range of 10^{-9} to 10^{-1} mho (stated accuracy $\pm$ 0.2%). The bridge circuit is shown in Figure 6. An internal oscillator adjusted to 1592 $\pm$ 1% cps ($\omega = 10^4$ rad/ sec) provides the source voltage. A buffer amplifier isolates the oscillator from the bridge circuits, to which four-terminal connections can be made. The detector is a tuned two-stage amplifier with a double-shadow "magic eye" associated with each stage. Balance of the unknown impedance is made against standards of conductance and capacitance in parallel. Tappings on the two bridge transformers, connected to decade controls, permit measurements to be made accurately over a wide range of impedance. Because of the unique design of the bridge, the impedance of the sample leads is automatically eliminated. At balance, no potential exists across the detector primary; hence it is possible to connect an impedance between the right-hand terminal of the unknown and neutral without affecting the accuracy of the measurement. Similarly, connecting an impedance between the left-hand terminal of the unknown and neutral merely reduces the voltage supplied to both the unknown and the standards in proportion to the turns ratio. It is possible therefore, to measure the sample impedance in situ without having to make corrections for parallel lead impedance. Series resistance of the leads does introduce

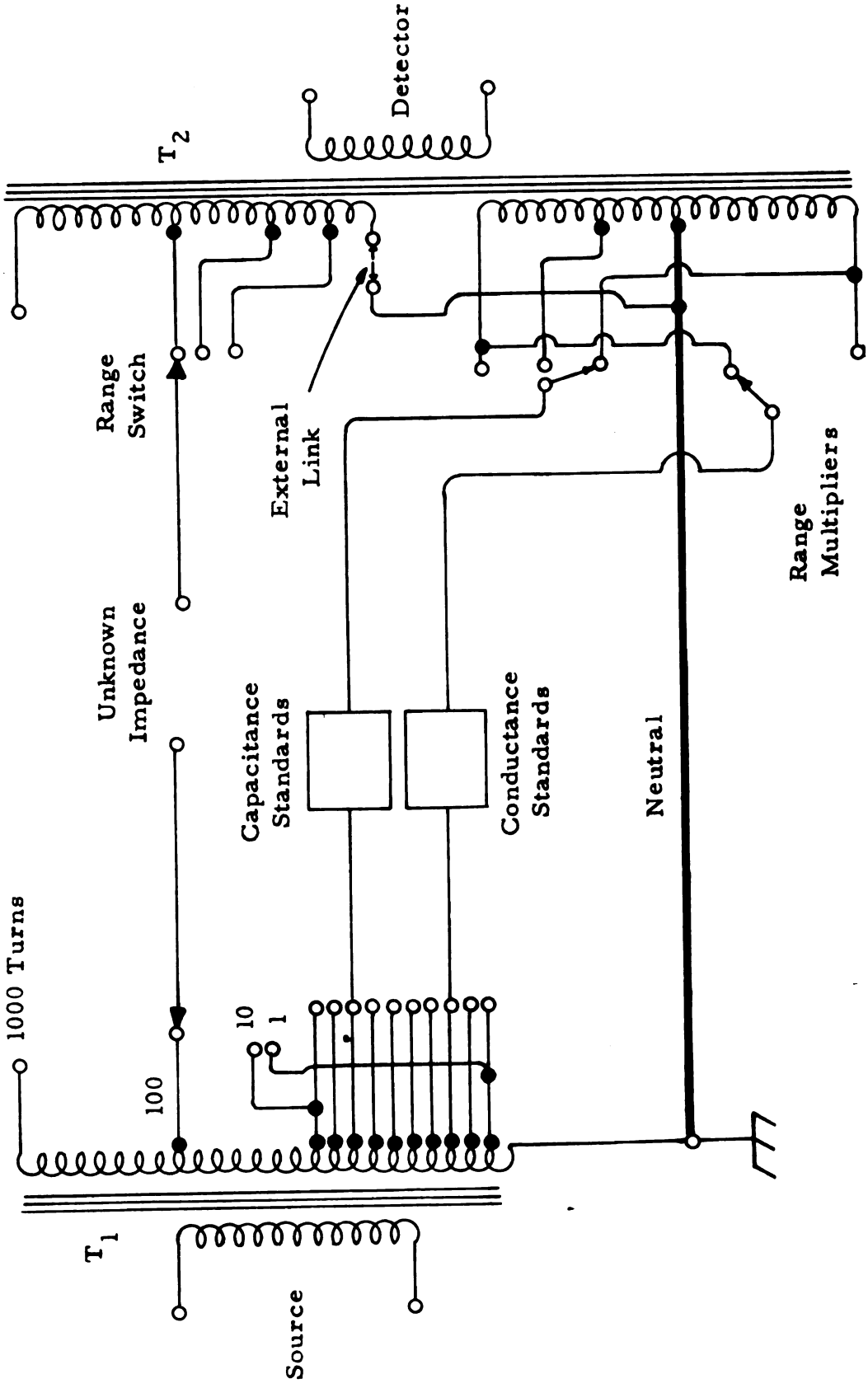

Fig. 6 - ac bridge circuit

an error, but this error is negligible for sample resistances greater than 100 ohms.

The Wayne Kerr Universal Bridge was also used for measuring electrical conductivity at frequencies from 50 to 20,000 cps by connecting an external source and detector. The principle of operation is the same, except that the internal bridge oscillator and detector are switched off. The external frequency source was a Hewlett-Packard Audio Oscillator Model 201B having a frequency range of 20 to 20,000 cps and a calibration accuracy of $\pm$ 2%. A General Radio Tuned Amplifier and Null Detector, type 1232-A, having the same frequency range as the audio oscillator, was used as a null detector for the signal. The conductivity of all of the single crystal samples was found to be independent of frequency in the temperature range of interest.

At high temperatures, where the sample impedance became less than about 100 ohms, it was necessary to use a guarded dc method to measure the conductivity. Figure 7 is a diagram of the dc measuring circuit. The source of constant voltage is a Keithley model 240 regulated high-voltage supply with a range of $\pm$ 0 to 1000 volts in one-volt steps (stated accuracy within 1%, above 10 volts). The series resistor R_s is a one-megohm precision resistor. Since the sample resistance during dc measurements is always less than 100 ohms, the current in the circuit is constant to better than one part in 10^4. The voltage drop across the sample is recorded on a Leeds and Northrup Speedomax H Adjustable Zero-Adjustable Range (AZAR) Recorder having a range of 0.67 to 100

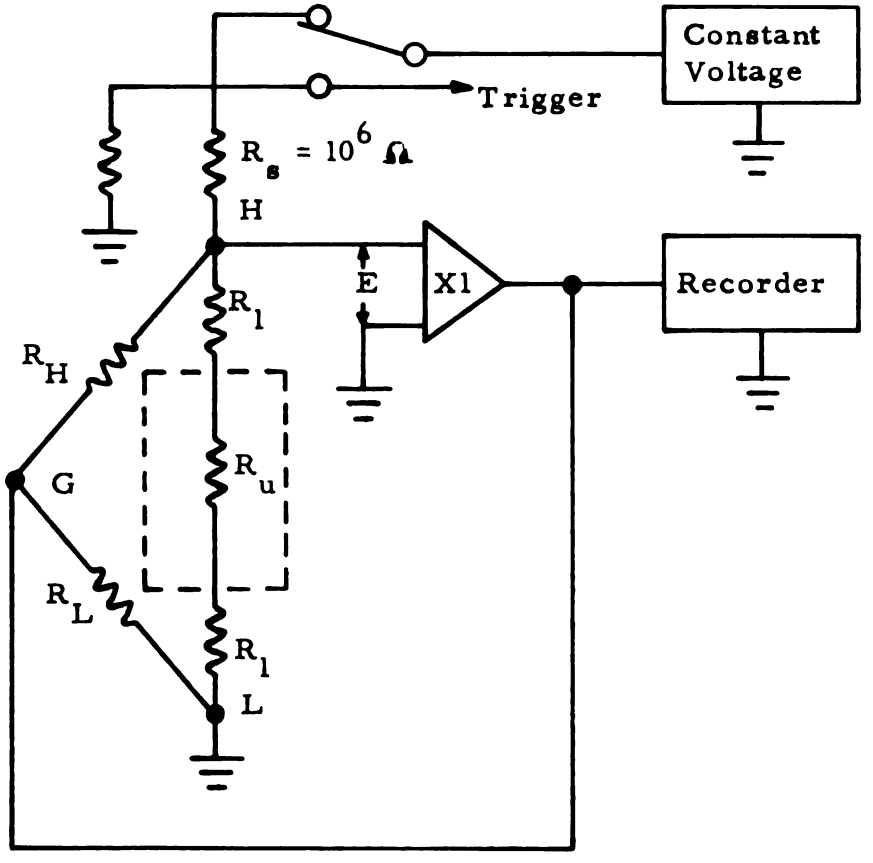

$$R_s >> R_u$$

$$I = v/R_s$$

Fig. 7 - dc circuit

millivolts full scale and a zero suppression of ± 50 millivolts (stated limit of error 0.3% of range span). The X1 amplifier is a Kintel model 112A-B unity-gain plug-in instrument with an input impedance of 10^{10} ohms and a gain stability of 0.001%. Its purpose is to keep the guard electrode at the same potential as the high side of the sample, thereby causing R_H to appear as an infinite impedance. This procedure insures that all of the current flowing through R_s flows through the sample R_u, and that the voltage at the X1 amplifier is just the voltage across the sample. The resistances R_H and R_L represent leakage resistance from the upper and lower electrodes to the guard electrode.

The lead resistance R_l, part of which is in the hot zone of the furnace, was measured as a function of temperature by bringing the upper and lower platinum electrodes of the sample holder into contact (no sample) and determining the resistance by the method just described. Figure 8 is a plot of the lead-wire correction over the temperature range 400 to 1400°C. The data points are for equilibrium temperatures and are accurate to ± 0.02 ohm.

The sample temperature was measured by means of two platinum vs platinum + 10% rhodium thermocouples built into the sample holder. The thermocouples were made from Engelhard standard-grade 0.020-inch thermocouple wire. A reference temperature of 0°C was maintained by a mixture of crushed ice and water. The thermocouple emf was measured on a Leeds and Northrup 8686 Millivolt Potentiometer having a range of -10.1 to +100.1 millivolts and a limit of error of

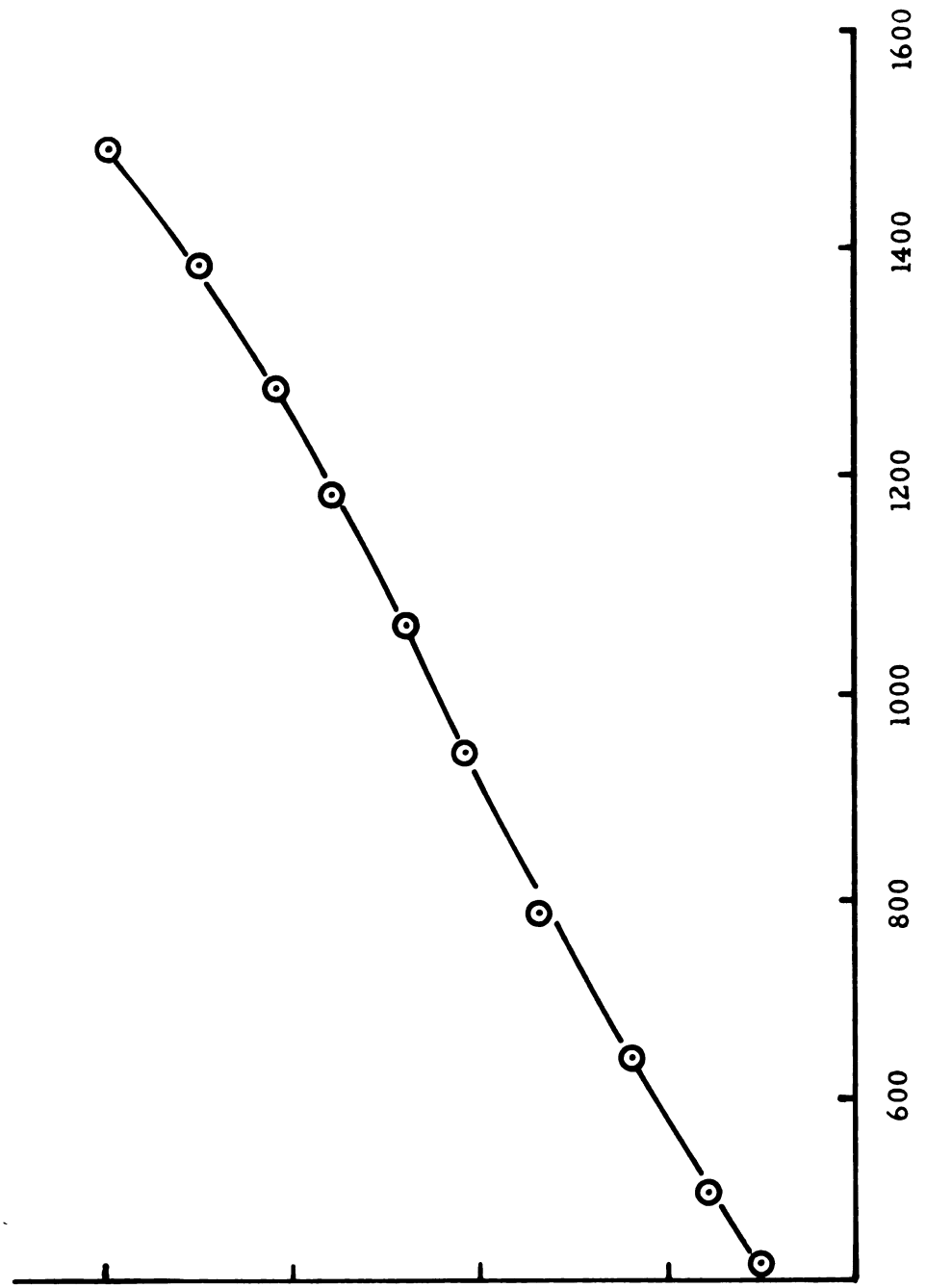

Fig. 8 - dc lead wire resistance correction

$\pm$ 0.05% of the reading $\pm$ 3 microvolts. The sample temperature was taken as the average of the readings of the upper and lower thermocouples.

An attempt was made to calibrate the thermocouples relative to each other at the same time that the dc lead-wire calibration was run. However, the results of two consecutive runs showed a small drift in the relative calibration. Walker et al[16] have found evidence of thermoelectric instability of some noble-metal thermocouples operating for long times at temperatures above 1000°C. They attribute this instability to contamination of the thermoelements by impurities, predominantly iron, from the ceramic protection tubes. Since this instability is cumulative with respect to both temperature and time, a relative calibration of the thermocouples cannot be considered dependable over long periods of time. Fortunately this uncertainty will not significantly affect the electrical-conductivity measurements since the analysis is made in terms of the absolute temperature and the relative error is small. For the same reasons, the absolute values were determined directly from a Leeds and Northrup thermocouple conversion table without calibration. On the basis of Walker's results and the experimental procedure followed here, the error is assumed to be negligible.

C. Experimental Procedure

Before any electrical measurements were made, the samples were heated to approximately 1200°C in the experimental apparatus for a period of two hours at an oxygen pressure of one atmosphere in an

effort to reach equilibrium with the surrounding gas. The results of the equilibration attempts are described in part V.

The temperature dependence of the electrical conductivity at constant pressure was measured by holding the oxygen partial pressure constant in the sample chamber and varying the sample temperature from 600 to 1400°C. The oxygen-pressure dependence of the conductivity was observed by repeating this procedure at several different partial pressures. The samples were equilibrated at 1200°C each time the oxygen pressure was changed. Measurements were made with the dc apparatus when the sample resistance was less than about 100 ohms. The data for the temperature variation of the conductivity at constant pressure were quite reproducible. The magnitude of the conductivity at constant temperature and variable pressures was less reproducible.

III. THEORETICAL CONSIDERATIONS

Chromium sesquioxide, Cr_2O_3, has the corundum structure with the point group symmetry class $\bar{3}$ (2/m) of the rhombohedral crystal system. This structure can also be described in the hexagonal system for ease of calculation. The hexagonal lattice parameters at room temperature[17, 18] are given in Table II.

Table II - Lattice parameters for Cr_2O_3 at 25°C.

a	c	c/a
4.96Å	13.59Å	2.74

Geometrically, the structure can be visualized as oxygen ions arranged in hexagonal-close-packed layers with two-thirds of the octahedral interstices between each layer containing chromium ions. Located along the threefold axis are pairs of distorted, cation-occupied octahedra that share a common face. In the basal plane these octahedra share a common edge with three similar octahedra. The corundum structure is shown schematically in Figure 9.

Chromia is antiferromagnetic below about 35°C with the spin directions alternating from one cation layer to the next (vis. + - + - along the c-axis[19]). However, the Néel temperature is low enough that even with the assumption of short-range order above T_N, the influence of spin coupling at 1000°C can be neglected.

The model assumed for the electronic structure of a 3d transition-metal oxide is similar to that of the usual semiconductor in that an empty

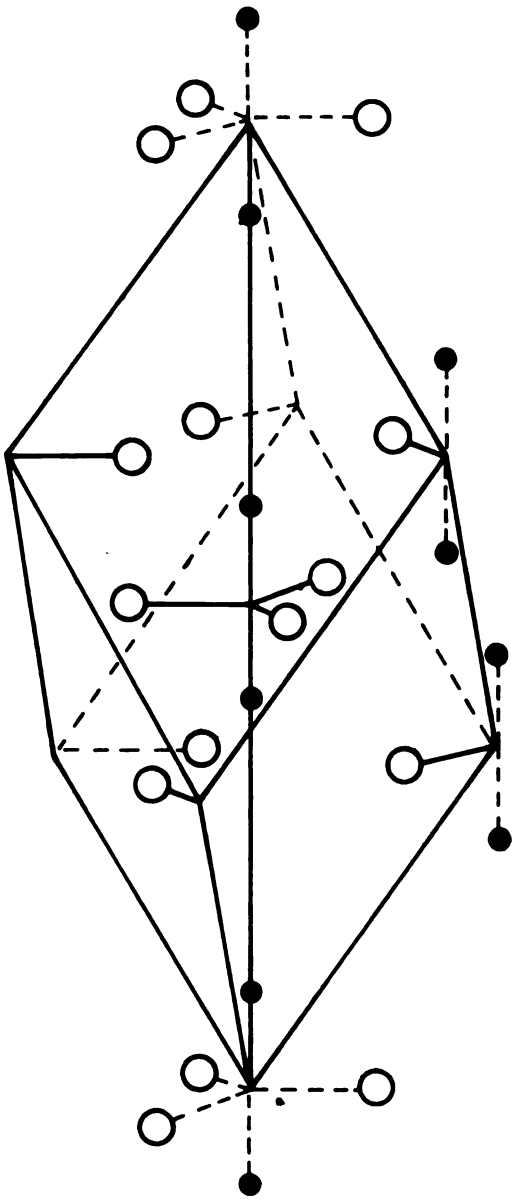

Fig. 9 - The corundum structure

conduction band is assumed to arise from the cation 4s levels, and a full valence band to arise from the anion (in this case oxygen) 2p levels. In addition, however, the 3d energy levels exist with some of them presumably located in the band gap. Although the possibility exists that the 3d wave functions may overlap sufficiently to form a very narrow band, there is no evidence for this overlap at present. Hence the 3d states will be discussed in terms of localized levels. In the case of chromia, the Cr^{3+} ion has three 3d electrons remaining outside the last closed-shell configuration. Electronic transport may result from the motion of charge carriers in the bands or in the localized levels or in both simultaneously.

The possible "intrinsic" mechanisms for production of electronic charge carriers in Cr_2O_3 are

$$O^{2-} \rightarrow O^{1-} + \text{4s electron} \qquad \text{(III-1)}$$

$$O^{2-} + Cr^{3+} \rightarrow O^{1-} + Cr^{2+} \qquad \text{(III-2)}$$

$$Cr^{3+} \rightarrow Cr^{4+} + \text{4s electron} \qquad \text{(III-3)}$$

$$2Cr^{3+} \rightarrow Cr^{2+} + Cr^{4+} \qquad \text{(III-4)}$$

These reactions represent (1) the formation of an electron-hole pair by excitation of an electron from the valence band to the conduction band, (2) the formation of a hole in the oxygen 2p band and an electron in the 3d levels, (3) the excitation of an electron to the 4s band leaving a hole in the 3d levels, and (4) the formation of an electron-hole pair in the 3d levels. The term "intrinsic" will be used here to describe those

processes which are unaffected by external influence, in particular by changes in the defect structure brought about by deviations from stoichiometry.

In addition to the intrinsic reactions mentioned, there are a large number of possible defect reactions which could be written to account for the electrical conductivity. Of the reactions available the most likely one is

$$(3/4)O_2^{(g)} \rightleftharpoons (3/2)O_{lat} + V_{Cr}^{3-} + 3\oplus \qquad \text{(III-5)}$$

where $O_2^{(g)}$ = gaseous oxygen

O_{lat} = oxygen ion on a lattice site

V_{Cr}^{3-} = triply-ionized Cr vacancies

$\oplus$ = positive-charge carrier (hole).

From the theory of the thermodynamics of defects[20] the concentrations of the various quantities can be expressed by the equilibrium equation

$$\left[V_{Cr}^{3-}\right]\left[\oplus\right]^3 / P_{O_2}^{3/4} = K$$

where $\left[V_{Cr}^{3-}\right]$ = concentration of Cr vacancies

$\left[\oplus\right]$ = concentration of holes

P_{O_2} = partial pressure of oxygen

K = equilibrium constant.

Since there are three holes for every vacancy the concentration of holes

will be given by

$$\left[\oplus\right]^4 = K' P_{O_2}^{3/4}$$

or

$$\left[\oplus\right] = K' P_{O_2}^{3/16}.$$

The electrical conductivity is related to the concentration of charge carriers by the relation

$$\sigma = |e| \mu \left[\oplus\right] \qquad \text{(III-6)}$$

where σ = electrical conductivity

e = electronic charge

μ = mobility.

If equation (III-5) were the predominant source of charge carriers, then the relation

$$\sigma \propto P_{O_2}^{3/16} \qquad \text{(III-7)}$$

should hold. As mentioned previously, this pressure dependence has not been observed in conductivity experiments. However, recent measurements[21] of the self-diffusion of radioactive Cr^{51} in single crystals of Cr_2O_3 which were equilibrated with various damp hydrogen atmospheres at 1300°C have shown an oxygen-pressure dependence very close to that of equation (III-7). This evidence suggests that the reaction (III-5) is the correct defect reaction and that the ionic motion is not intrinsic at 1300°C.

These considerations eliminate the possibility of a predominant intrinsic mechanism due to charge production by thermally generated and ionized point defects (Schottky or Frenkel effect).

For an intrinsic mechanism of electron and hole production at equilibrium

$$\left[\ominus\right]\left[\oplus\right] \propto \exp\left(-E/kT\right)$$

and since $\left[\ominus\right] = \left[\oplus\right] = n$, the concentration of one type of carrier, then

$$n = A \exp\left(-E/2kT\right) \qquad \text{(III-8)}$$

where E = activation energy

k = Boltzmann's constant

T = absolute temperature,

and the constant A involves the change in entropy in the reaction. The electrical conductivity in this case can be written

$$\sigma = |e| \mu_e \left[\ominus\right] + |e| \mu_h \left[\oplus\right]$$

or using equation (III-8)

$$\sigma = |e| A \left(\mu_e + \mu_h\right) \exp\left(-E/2kT\right). \qquad \text{(III-9)}$$

The temperature dependence of the mobility depends very strongly on the conduction mechanism. The three intrinsic mechanisms described by equations (III-1), (III-2), and (III-3) involve charge transport in either the 2p or 4s band or both. Morin[5] suggests that the 2p band in oxides is between 10 and 20 ev wide, and that the mobility of holes in a band of this width should be quite high. Similar information for the 4s band is not available, but the mobility of electrons here should also be high; and for either case of broad-band conductivity it generally decreases as some negative power of the temperature[22]. For equation (III-4), which describes charge motion between the localized 3d levels, the mobility would be quite low and would increase exponentially with temperature. Experimental evidence for most transition-metal oxides leads to a mobility relation of the form

$$\mu \propto \exp(-h/kT).$$

The activation energy, h, is assumed to arise from the self-trapping of the charge carrier by the polarization it induces in the lattice around itself. For the case of intrinsic conductivity the charge carrier is assumed to exist as an excited state of a cation. The existence of an activated mobility leads to the concept of "hopping" of the charge carrier between equivalent lattice sites.

If it is assumed that the electron and hole mobilities are equal,

equation (III-9) reduces to

$$\sigma = |e| A' \exp\left[-(E/2 + h)/kT\right]. \qquad \text{(III-10)}$$

It has been suggested[2, 3] that "hopping" transport be treated as a diffusion process; in this case the constant A' would have a $1/T$ or perhaps even more complicated temperature dependence. For the temperature range of interest here, the exponential temperature dependence completely overcomes any simple linear term. Hence the analysis will be carried out in terms of equation (III-10).

IV. RESULTS AND ANALYSIS

A. Analytical Procedure

The data shall be described in the form

$$\sigma = \sigma_o \exp(-U/kT) \qquad \text{(IV-1)}$$

where σ = electrical conductivity in $(\text{ohm-cm})^{-1}$

U = activation energy in ev

k = Boltzmann's constant (8.622×10^{-5} ev/^{o}K)

T = absolute temperature in ^{o}K.

The data are taken in the form of an ac conductance G, or a dc voltage and current which, through Ohm's law, yield a resistance R. The sample is most conveniently considered as a resistance in parallel with a capacitance, but the bridge read-out is in terms of reciprocal resistance or conductance. The relationship between the ac conductance and the dc resistance is simply

$$G_p = 1/R_p . \qquad \text{(IV-2)}$$

The specific conductivity is related to the conductance by the relation

$$\sigma = Gt/A = Gt/\pi(d/2)^2 \qquad \text{(IV-3)}$$

where t = sample thickness in cm

A = electrode area in cm^2

d = electrode diameter in cm.

Taking the natural logarithm of both sides of equation (IV-1) yields

$$\ln \sigma = \ln \sigma_o - U/kT$$

or in terms of common logarithms

$$\log \sigma = \log \sigma_o - U/2.3\,kT . \qquad \text{(IV-4)}$$

Plotting $\log \sigma$ vs $1/T$ will give a straight line with slope $-U/2.3k$ and intercept $\log \sigma_o$. In practice $\log \sigma$ is plotted against $1000/T$ for convenience.

The method of least squares[23] is applied to obtain the numerical values of U and σ_o from the straight-line portions of the data. Equation (IV-4) has the form

$$y = a + bx$$

for which

$$b = (\bar{x}\bar{y} - \overline{xy})/(\bar{x}^2 - \overline{x^2}) \text{ and } a = \bar{y} - b\bar{x} \qquad \text{(IV-5)}$$

where the barred quantities in equations (IV-5) are arithmetic means. The probable errors are calculated from the relations

$$P_b = r_e\sqrt{(n/D)} \qquad \text{and} \qquad P_a = r_e\sqrt{(\Sigma x_i^2/D)}$$

where $r_e = 0.6745 \sqrt{\left[\Sigma d_i^2/(n-2)\right]}$

$D = n\Sigma x_i^2 - (\Sigma x_i)^2$

$d_i = y_i - (a + bx_i)$.

The experimental data for four single-crystal samples are presented in Tables III through VI. The abbreviated column headings for the tables of data are defined as follows:

UTC = upper thermocouple reading in mv

LTC = lower thermocouple reading in mv

Temp = average temperature in ^{o}C

$10^3/T$ = reciprocal absolute temperature in $^{o}K^{-1} \times 10^3$

I = dc current in μa

V = dc voltage in μv

G = conductance in millimho (1/ ohm) x 10^{-3}

B. Sample 3SC - Unoriented Single Crystal

Table III contains the experimental data for the electrical conductivity of an unoriented single crystal sample of pure Cr_2O_3 over the temperature range 569 to 1215^{o}C for two oxygen pressures. The sample thickness was 0.156 cm and the electrode diameter was 0.37 cm. The log of the conductivity is then, by equation (IV-3),

$$\log \sigma = \log G + 0.162.$$

Figure 10 is a plot of log σ vs 1/ T for sample 3SC.

Table III - Experimental data for sample 3SC.

UTC (mv)	LTC (mv)	Temp (^{o}C)	$10^{3}/T$ (^{o}K)$^{-1}$	G (mM)	log σ
		P_{O_2} = 1 atm			
10.124	10.057	1045	0.759	9.057	-1.881
9.341	9.286	978	0.799	5.000	-2.139
8.654	8.611	918	0.840	3.311	-2.318
8.219	8.181	879	0.868	2.706	-2.406
7.473	7.447	812	0.922	2.036	-2.529
6.655	6.643	737	0.990	1.494	-2.664
5.874	5.874	663	1.068	0.9786	-2.847
4.905	4.920	569	1.188	0.4255	-3.209
5.300	5.309	608	1.135	0.6157	-3.049
6.199	6.194	694	1.034	1.190	-2.762
6.938	6.922	763	0.965	1.672	-2.615
9.732	9.669	1011	0.779	6.634	-2.016
10.469	10.393	1074	0.742	11.93	-1.761
8.302	8.264	887	0.862	2.818	-2.388
10.279	10.176	1057	0.752	9.869	-1.844
11.028	10.906	1119	0.718	17.96	-1.584
		P_{O_2} = 10^{-2} atm			
12.182	12.050	1215	0.672	40.20	-1.234

Table III - Continued

UTC (mv)	LTC (mv)	Temp (^{o}C)	$10^{3}/T$ ($^{o}K)^{-1}$	G (mM)	log σ
10.214	10.127	1052	0.755	8.880	-1.890
9.038	8.972	951	0.817	3.609	-2.281
7.720	7.679	834	0.903	1.790	-2.585
6.458	6.431	718	1.009	0.9375	-2.866
5.445	5.428	621	1.119	0.4196	-3.215
4.990	4.974	576	1.178	0.2650	-3.415
5.900	5.879	665	1.066	0.6221	-3.044
7.010	6.978	769	0.960	1.277	-2.732
8.030	7.985	862	0.881	2.064	-2.523
8.662	8.604	918	0.840	2.856	-2.382
9.599	9.520	999	0.786	5.394	-2.106
10.493	10.396	1075	0.742	11.18	-1.790
7.392	7.356	804	0.929	1.606	-2.632
		P_{O_2} = 1 atm			
7.398	7.361	805	0.928	1.624	-2.627
8.586	8.522	911	0.845	2.835	-2.385
9.500	9.416	990	0.792	5.130	-2.128
7.336	7.298	799	0.933	1.603	-2.633
10.113	10.015	1043	0.760	8.396	-1.914
11.885	11.745	1190	0.684	33.87	-1.308
8.761	8.688	926	0.834	3.228	-2.329

Table III - Continued

UTC (mv)	LTC (mv)	Temp (^{o}C)	$10^{3}/T$ (^{o}K)$^{-1}$	G (mM)	log σ
12.092	11.950	1207	0.676	39.17	-1.245
8.745	8.675	925	0.835	3.175	-2.336
7.263	7.225	792	0.939	1.530	-2.653
6.114	6.094	685	1.044	0.8225	-2.923
		$P_{O_2} = 10^{-a}$ atm			
12.191	12.060	1216	0.672	40.92	-1.226
9.424	9.353	984	0.796	4.733	-2.163
8.363	8.310	891	0.859	2.380	-2.461
7.357	7.315	801	0.931	1.446	-2.678
6.208	6.185	694	1.034	0.7342	-2.972
5.029	5.015	580	1.172	0.2650	-3.415
5.594	5.574	635	1.101	0.4452	-3.189
6.977	6.943	766	0.962	1.187	-2.764

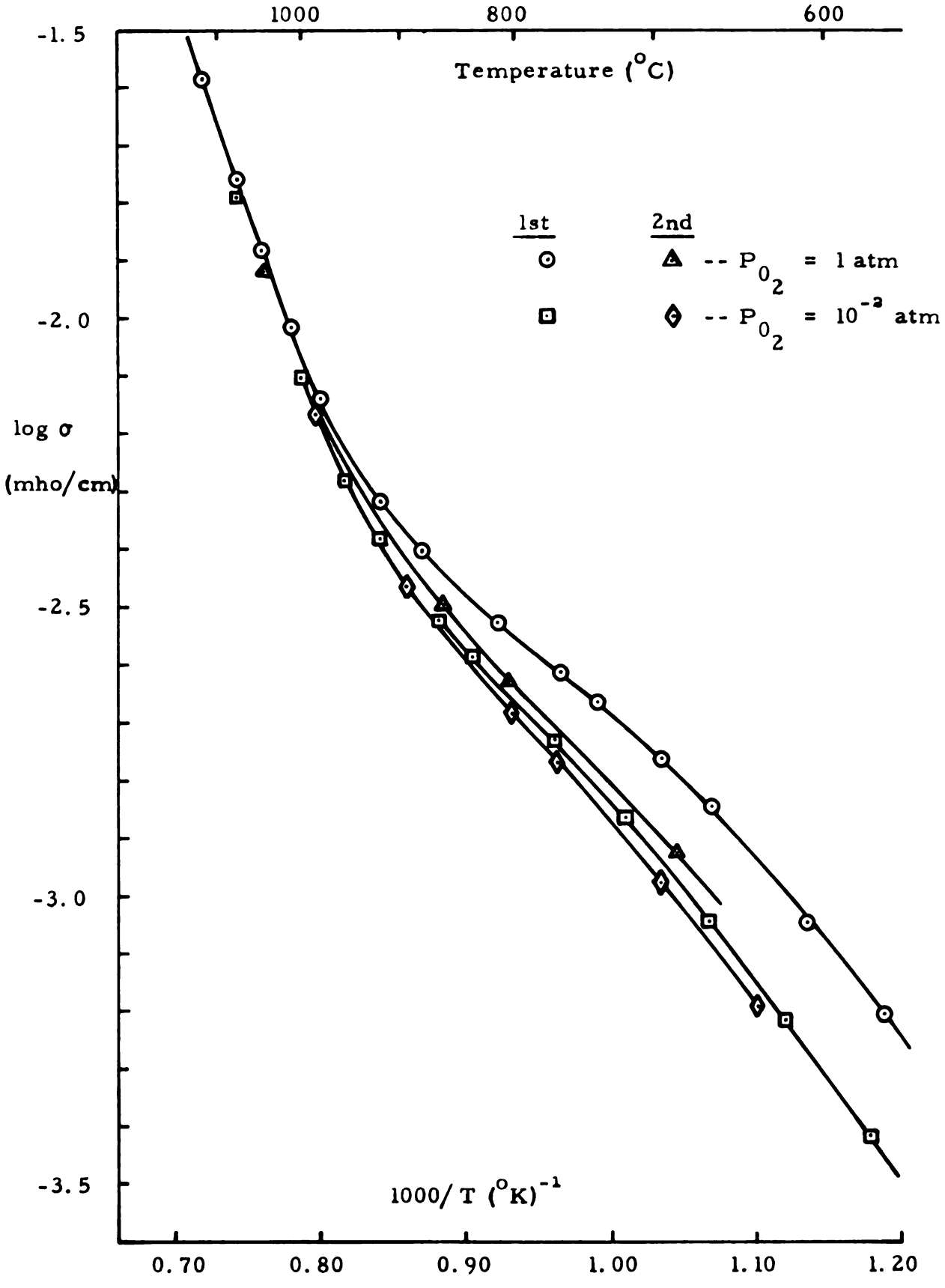

Fig. 10 - Electrical conductivity of sample 3SC

C. Sample 2SC - Unoriented Single Crystal

Table IV contains experimental data for the electrical conductivity of a second single-crystal sample of Cr_2O_3 cut from the same boule and having the same unspecified orientation as sample 3SC. These data cover a temperature range of 686 to 1416°C for two oxygen pressures. The sample thickness was 0.155 cm and the electrode diameter was 0.37 cm. The log of the conductivity is given by

$$\log \sigma = \log G + 0.158.$$

Figure 11 is a plot of log σ vs 1/T for sample 2SC.

The data in Table IV which are marked with an asterisk were used in a least-squares analysis to obtain the values of E and σ_o for equation (IV-1) in the high-temperature, straight-line region of the conductivity curve. The results for sample 2SC was

$$\sigma = (1.48 \pm 0.10) \times 10^4 \exp\left[-(1.63 \pm 0.01 \text{ ev})/kT\right]$$

in the temperature range 1115 to 1416°C. Figure 12 is a plot of the experimental points on the least-squares line.

Table IV - Experimental data for sample 2SC.

UTC (mv)	LTC (mv)	Temp (^{o}C)	$10^3/T$ ($^{o}K)^{-1}$	I (μa)	V (μv)	G (mM)	log σ
			P_{O_2} = 1 atm				
14.549	14.500	1416	0.592	50.0	432	141.0	-0.693*
13.974	13.930	1368	0.609	40.0	454	102.0	-0.833*
13.473	13.431	1326	0.625	30.0	442	75.8	-0.962*
13.043	13.016	1291	0.639	20.0	380	57.2	-1.085*
12.354	12.323	1234	0.664	20.0	581	36.3	-1.282*
11.657	11.634	1176	0.690	20.0	938	22.0	-1.500*
10.923	10.909	1115	0.720	10.0	816	12.5	-1.745*
10.141	10.135	1049	0.756	----	---	6.735	-2.014
8.959	8.970	947	0.820	----	---	2.892	-2.381
8.080	8.102	869	0.876	----	---	1.850	-2.575
7.276	7.312	797	0.935	----	---	1.266	-2.740
6.083	6.141	686	1.043	----	---	0.5770	-3.081
6.960	7.011	768	0.961	----	---	1.065	-2.815
7.914	7.952	855	0.887	----	---	1.718	-2.607
8.795	8.822	933	0.829	----	---	2.634	-2.421
9.364	9.379	983	0.796	----	---	3.750	-2.268
9.812	9.815	1021	0.773	----	---	5.200	-2.126
10.360	10.350	1067	0.746	----	---	7.992	-1.939
11.053	11.036	1126	0.715	----	---	13.79	-1.702*

Table IV - Continued

UTC (mv)	LTC (mv)	Temp (^{o}C)	$10^{3}/T$ (^{o}K)$^{-1}$	I (μa)	V (μv)	G (mM)	log σ
11.900	11.873	1196	0.681	20.0	796	26.1	-1.425*
12.610	12.572	1255	0.654	20.0	497	42.8	-1.211*
13.584	13.537	1335	0.622	30.0	419	80.5	-0.936*
11.492	11.467	1162	0.697	10.0	533	19.3	-1.557*
8.652	8.670	920	0.838	----	---	2.355	-2.470
			$P_{O_2} = 10^{-2}$ atm				
13.624	13.555	1338	0.621	30.0	422	79.8	-0.940
12.636	12.581	1256	0.654	20.0	499	42.7	-1.212
11.579	11.536	1169	0.693	15.0	773	20.0	-1.541
10.666	10.634	1092	0.733	----	---	9.720	-1.854
9.728	9.706	1013	0.778	----	---	4.628	-2.177
8.706	8.696	924	0.835	----	---	2.417	-2.459
7.749	7.758	839	0.899	----	---	1.583	-2.643

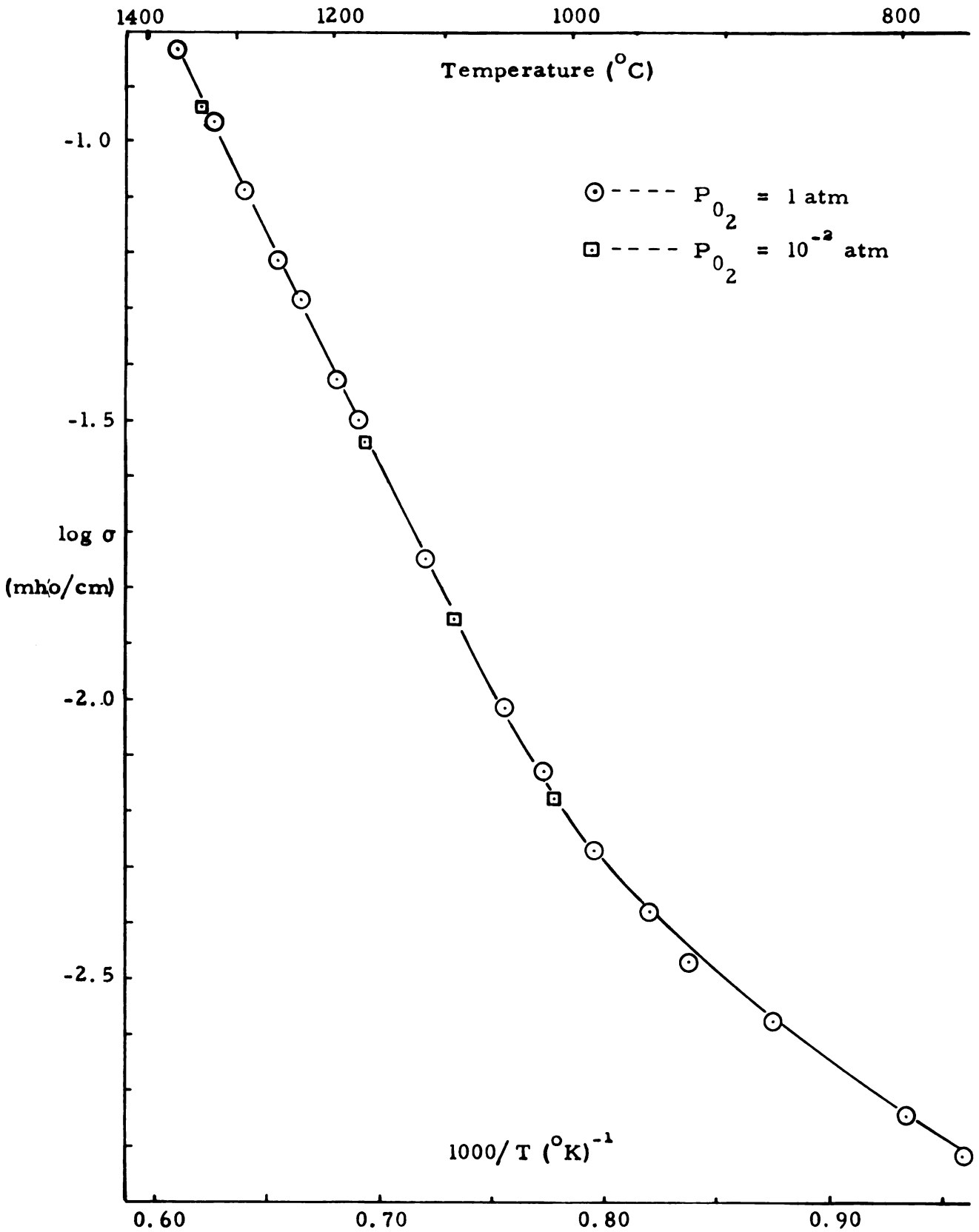

Fig. 11 - Electrical conductivity of sample 2SC

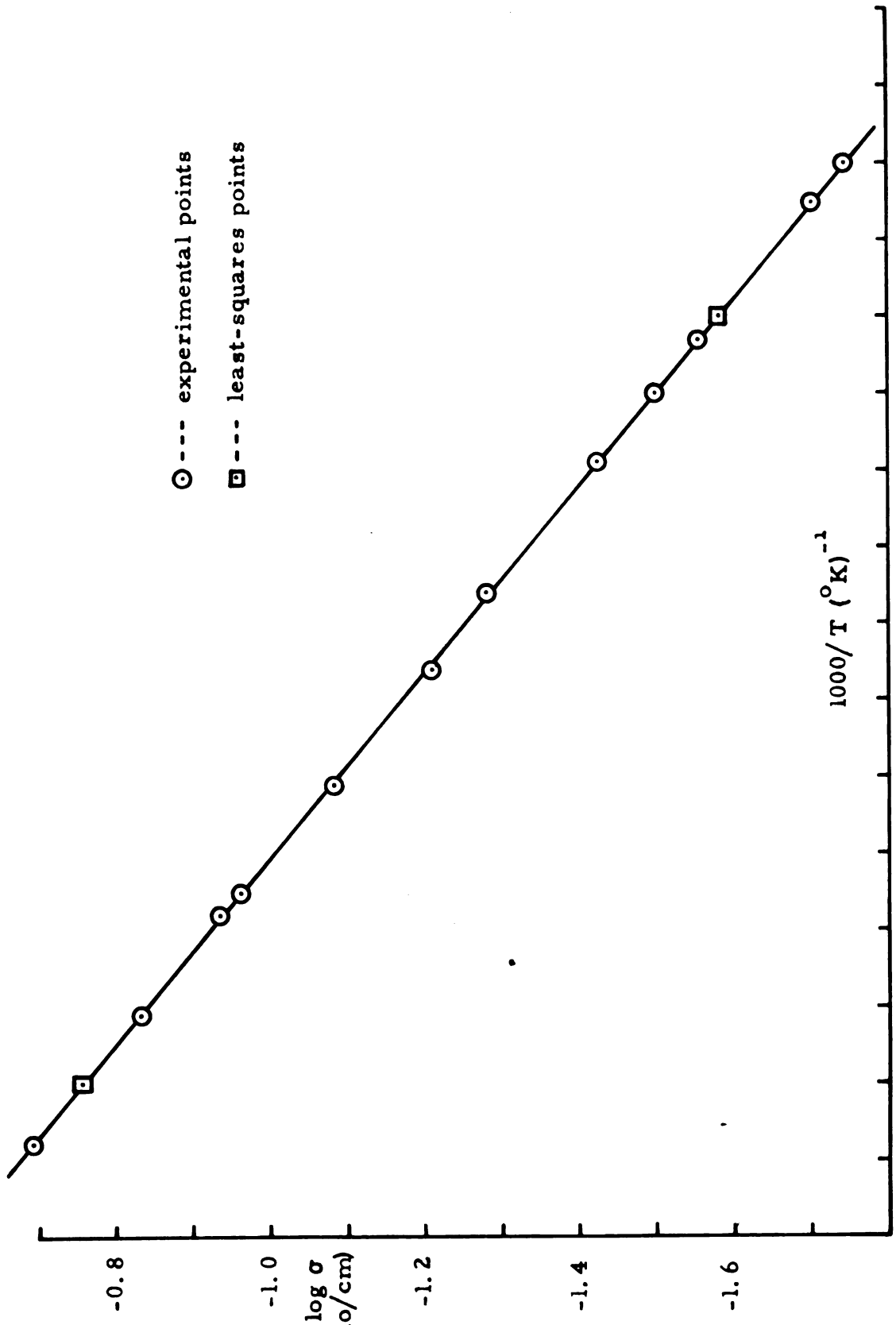

Fig. 12 - Least-squares line for sample 2SC

D. Sample 4SC(a) - Oriented Single Crystal

Table V contains experimental data for the electrical conductivity of a single-crystal sample of Cr_2O_3 oriented so that the current passes through it in a direction perpendicular to the c-axis. These data cover a temperature range of 887 to 1392°C for two oxygen pressures. The sample thickness was 0.269 cm and the electrode diameter was 0.35 cm. The log of the conductivity is given by

$$\log \sigma = \log G + 0.447.$$

Figure 13 is a plot of log σ vs $1/T$ for sample 4SC(a).

The data in Table V which are marked with an asterisk were used in a least-squares analysis for the high-temperature, straight-line, region of the conductivity curve. The result for sample 4SC(a) was

$$\sigma = (1.96 \pm 0.16) \times 10^4 \exp\left[-(1.68 \pm 0.01 \text{ ev})/kT\right]$$

in the temperature range 1278 to 1392°C. Figure 14 is a plot of the experimental points on the least-squares line.

Table V - Experimental data for sample 4SC(a).

UTC (mv)	LTC (mv)	Temp (^{o}C)	$10^3/T$ ($^{o}K)^{-1}$	I (μa)	V (μv)	G (mM)	log σ
			P_{O_2} = 1 atm				
14.202	14.002	1380	0.605	30.0	588	55.4	-0.809
13.987	13.794	1363	0.611	30.0	661	48.8	-0.864
13.666	13.480	1336	0.622	30.0	790	40.3	-0.947
13.381	13.197	1313	0.631	25.0	779	33.8	-1.025
13.079	12.903	1288	0.641	20.0	742	28.1	-1.104
12.720	12.552	1258	0.653	15.0	690	22.5	-1.201
12.158	12.004	1212	0.673	10.0	642	15.9	-1.350
11.764	11.620	1180	0.688	----	---	12.72	-1.449
11.299	11.163	1141	0.707	----	---	9.939	-1.556
10.880	10.758	1107	0.725	----	---	8.164	-1.641
10.354	10.242	1062	0.749	----	---	6.537	-1.738
9.172	9.089	962	0.810	----	---	4.268	-1.923
8.319	8.252	887	0.862	----	---	2.596	-2.139
9.291	9.199	972	0.803	----	---	3.940	-1.958
12.017	11.865	1201	0.678	10.0	715	14.3	-1.398
12.545	12.383	1244	0.659	15.0	793	19.5	-1.264
12.957	12.787	1278	0.645	20.0	829	25.0	-1.154*
13.249	13.072	1302	0.635	25.0	863	30.3	-1.072*
13.563	13.382	1328	0.625	30.0	855	37.1	-0.984*

Table V - Continued

UTC (mv)	LTC (mv)	Temp (^{o}C)	$10^3/T$ (^{o}K)$^{-1}$	I (μa)	V (μv)	G (mM)	log σ
13.889	13.700	1355	0.614	30.0	705	45.5	-0.895*
14.343	14.145	1392	0.601	30.0	551	59.5	-0.779*
13.996	13.803	1364	0.611	30.0	667	48.4	-0.869*
13.675	13.488	1337	0.621	30.0	804	39.6	-0.955*
13.392	13.210	1314	0.630	25.0	786	33.4	-1.029*
13.078	12.902	1288	0.641	20.0	759	27.5	-1.114*
12.628	12.461	1251	0.656	20.0	980	21.1	-1.230
11.935	11.791	1194	0.682	----	---	12.83	-1.445
			$P_{O_2} = 10^{-8}$ atm				
12.579	12.417	1247	0.658	----	---	19.64	-1.260
12.227	12.074	1218	0.671	----	---	15.21	-1.371
11.693	11.548	1174	0.691	----	---	10.69	-1.524
11.258	11.130	1138	0.709	----	---	8.053	-1.647
10.809	10.695	1101	0.728	----	---	6.076	-1.769
10.323	10.221	1060	0.750	----	---	4.586	-1.892
9.397	9.316	982	0.797	----	---	2.905	-2.090
8.319	8.259	887	0.862	----	---	1.798	-2.298

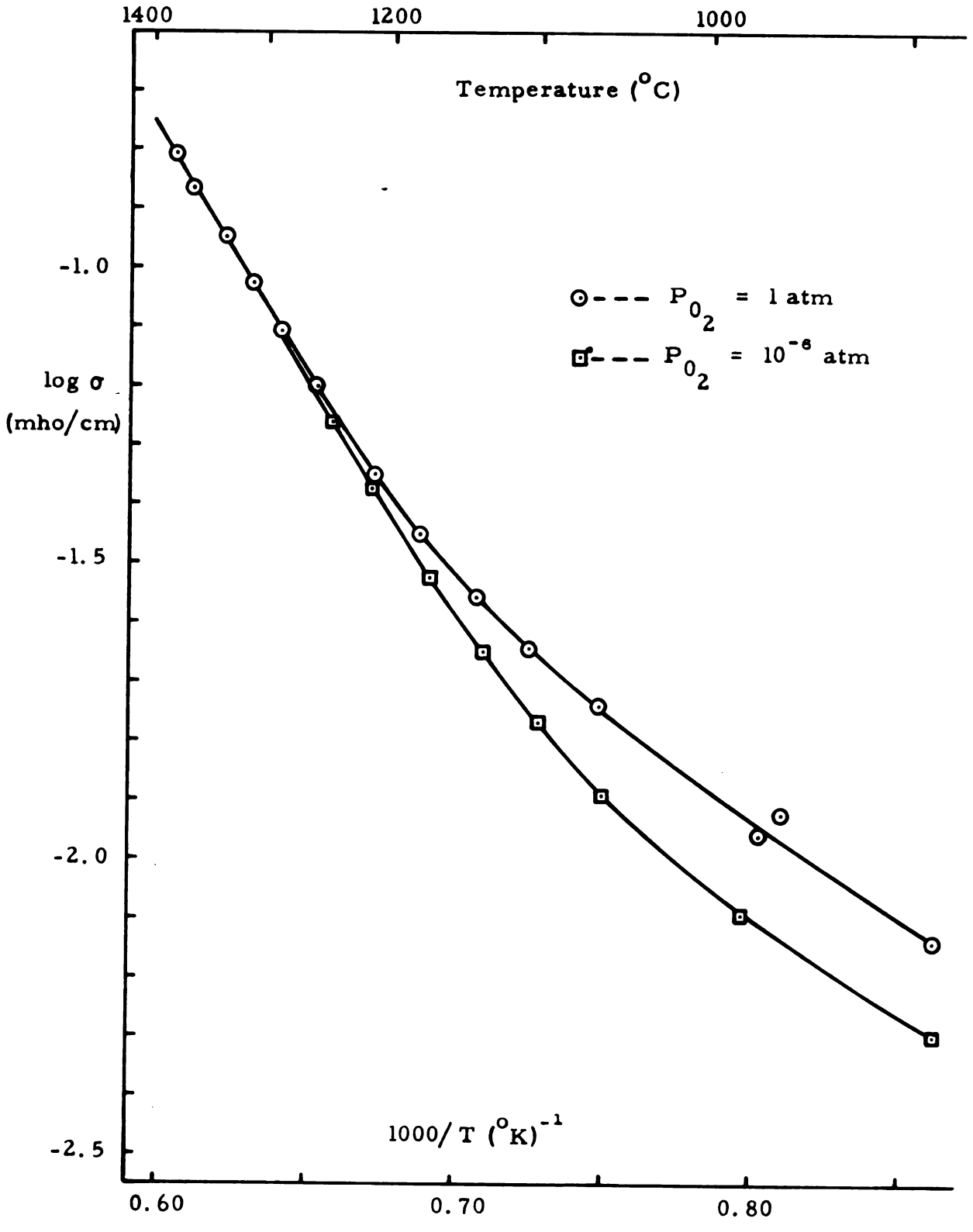

Fig. 13 - Electrical conductivity of sample 4SC(a)

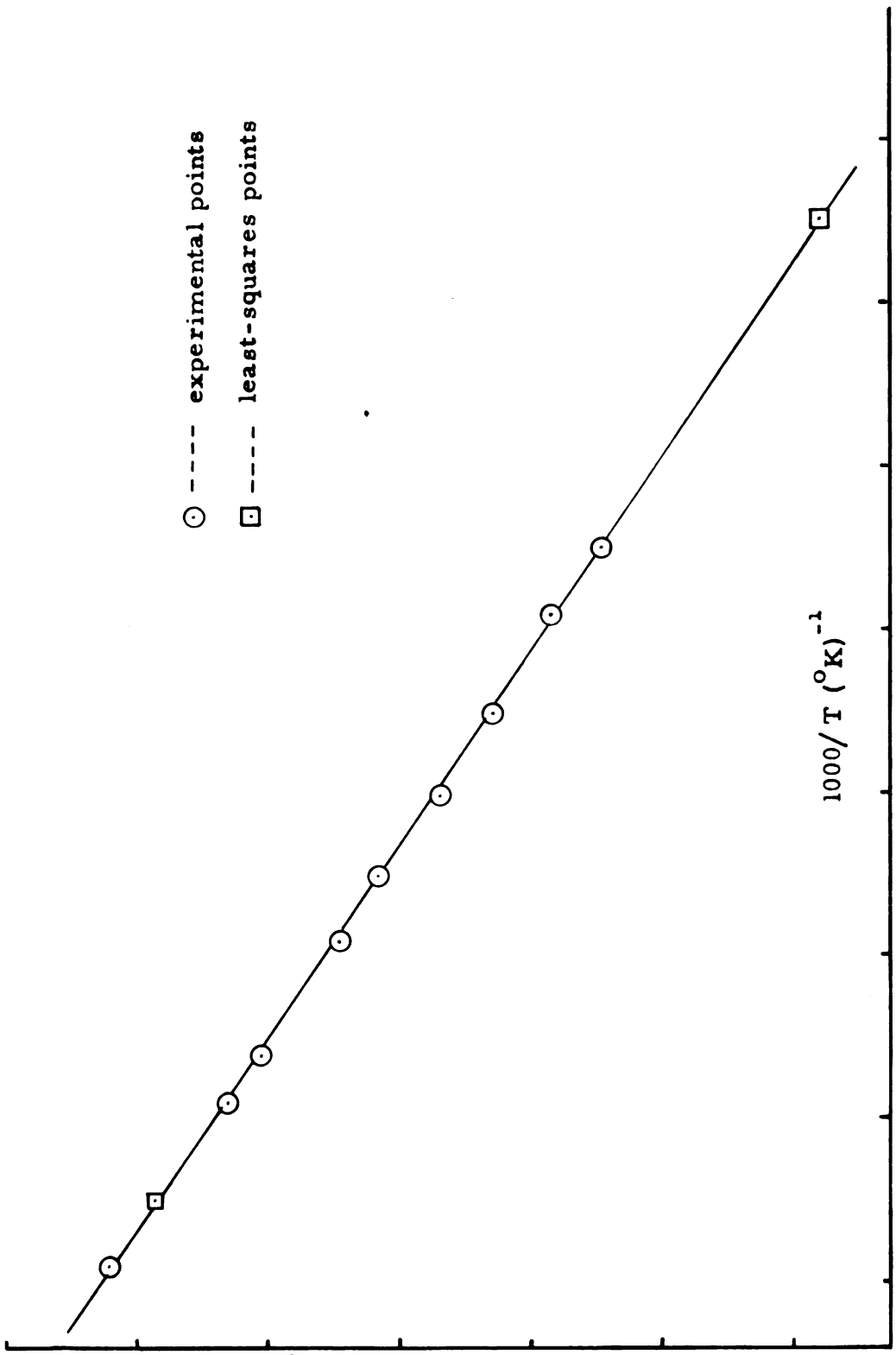

Fig. 14 - Least-squares line for sample 4SC(a)

E. Sample 4SC(c) - Oriented Single Crystal

Table VI contains experimental data for the electrical conductivity of a single crystal sample of Cr_2O_3 oriented so that the current passes through it in a direction parallel to the c-axis. These data cover a temperature range of 1087 to 1381°C for one oxygen pressure. The sample thickness was 0.195 cm and the electrode diameter was 0.28 cm. The log of the conductivity is given by

$$\log \sigma = \log G + 0.501$$

Figure 15 is a plot of log σ vs $1/T$ for sample 4SC(c).

The data in Table VI which are marked with an asterisk were used in a least-squares analysis for the high-temperature, straight-line region of the conductivity curve. The result for sample 4SC(c) was

$$\sigma = (1.37 \pm 0.15) \times 10^4 \exp\left[-(1.59 \pm 0.02 \text{ ev})/kT\right]$$

in the temperature range 1247 to 1334°C. Figure 16 is a plot of the experimental points on the least-squares line.

Table VI - Experimental data for sample 4SC(c).

UTC (mv)	LTC (mv)	Temp (^{o}C)	$10^{3}/T$ (^{o}K)$^{-1}$	I (μa)	V (μv)	G (mM)	log σ
			P_{O_2} = 1 atm				
13.959	13.785	1361	0.612	30.0	593	54.9	-0.760
13.625	13.456	1334	0.622	30.0	724	44.3	-0.853*
13.313	13.149	1308	0.633	30.0	872	36.3	-0.939*
13.060	12.903	1287	0.641	25.0	839	31.2	-1.005*
12.672	12.523	1255	0.654	20.0	844	24.6	-1.108*
12.197	12.058	1216	0.672	15.0	840	18.4	-1.235
11.787	11.659	1182	0.687	10.0	712	14.3	-1.342
11.299	11.179	1142	0.707	----	---	10.80	-1.466
10.640	10.534	1087	0.735	----	---	7.300	-1.636
11.198	11.074	1133	0.711	----	---	9.792	-1.508
11.724	11.590	1177	0.690	----	---	13.29	-1.375
12.042	11.902	1203	0.678	10.0	634	16.2	-1.291
12.578	12.431	1247	0.658	15.0	683	22.7	-1.143*
12.996	12.841	1282	0.643	20.0	708	29.5	-1.029*
13.271	13.108	1304	0.634	25.0	754	34.9	-0.956*
13.553	13.387	1328	0.625	30.0	769	41.5	-0.881*
13.929	13.757	1359	0.613	30.0	641	50.5	-0.796
14.203	14.027	1381	0.605	30.0	543	60.5	-0.718
13.884	13.714	1355	0.614	30.0	652	49.5	-0.804
13.570	13.405	1329	0.624	30.0	781	40.8	-0.888
13.276	13.115	1305	0.634	30.0	914	34.6	-0.961

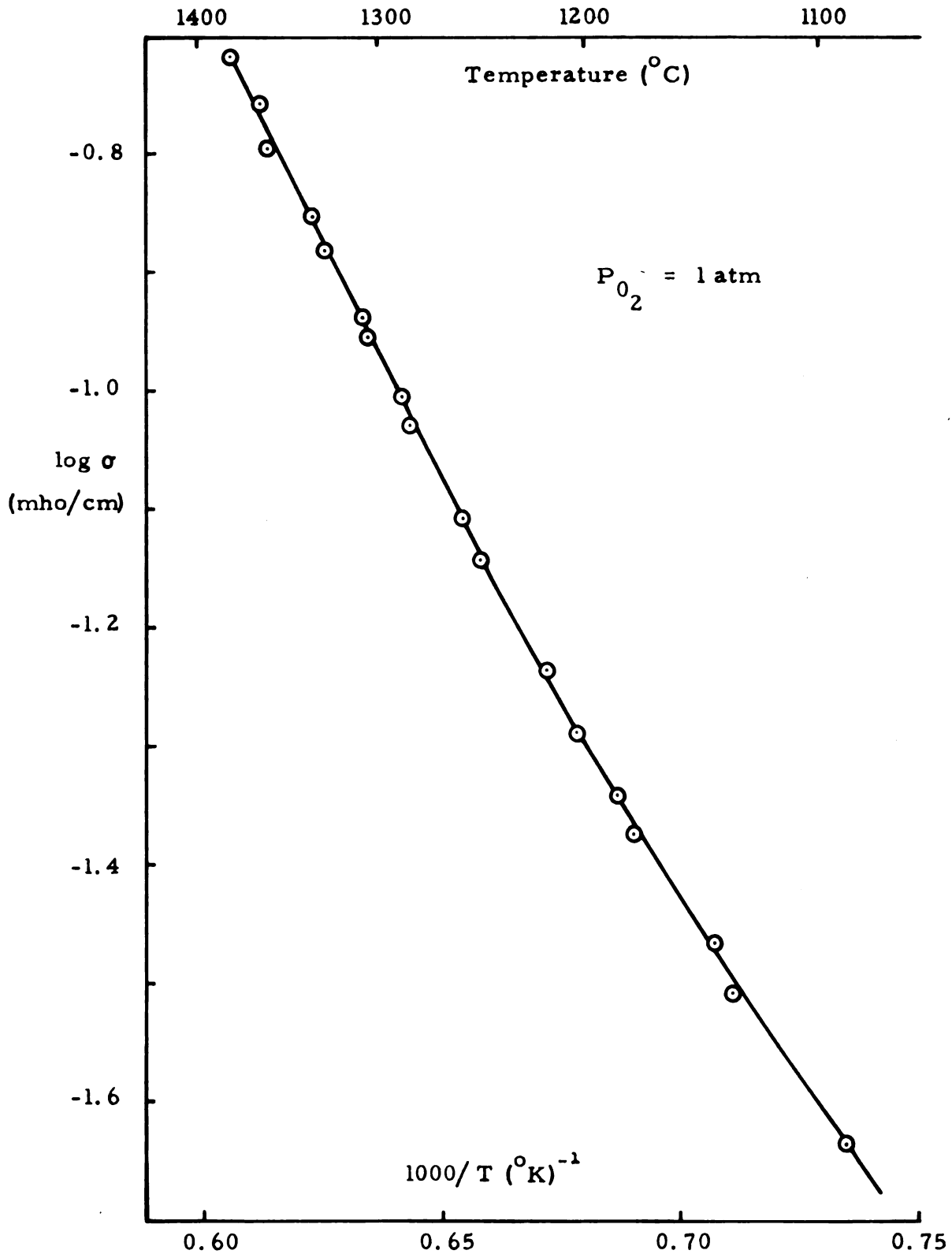

Fig. 15 - Electrical conductivity of sample 4SC(c)

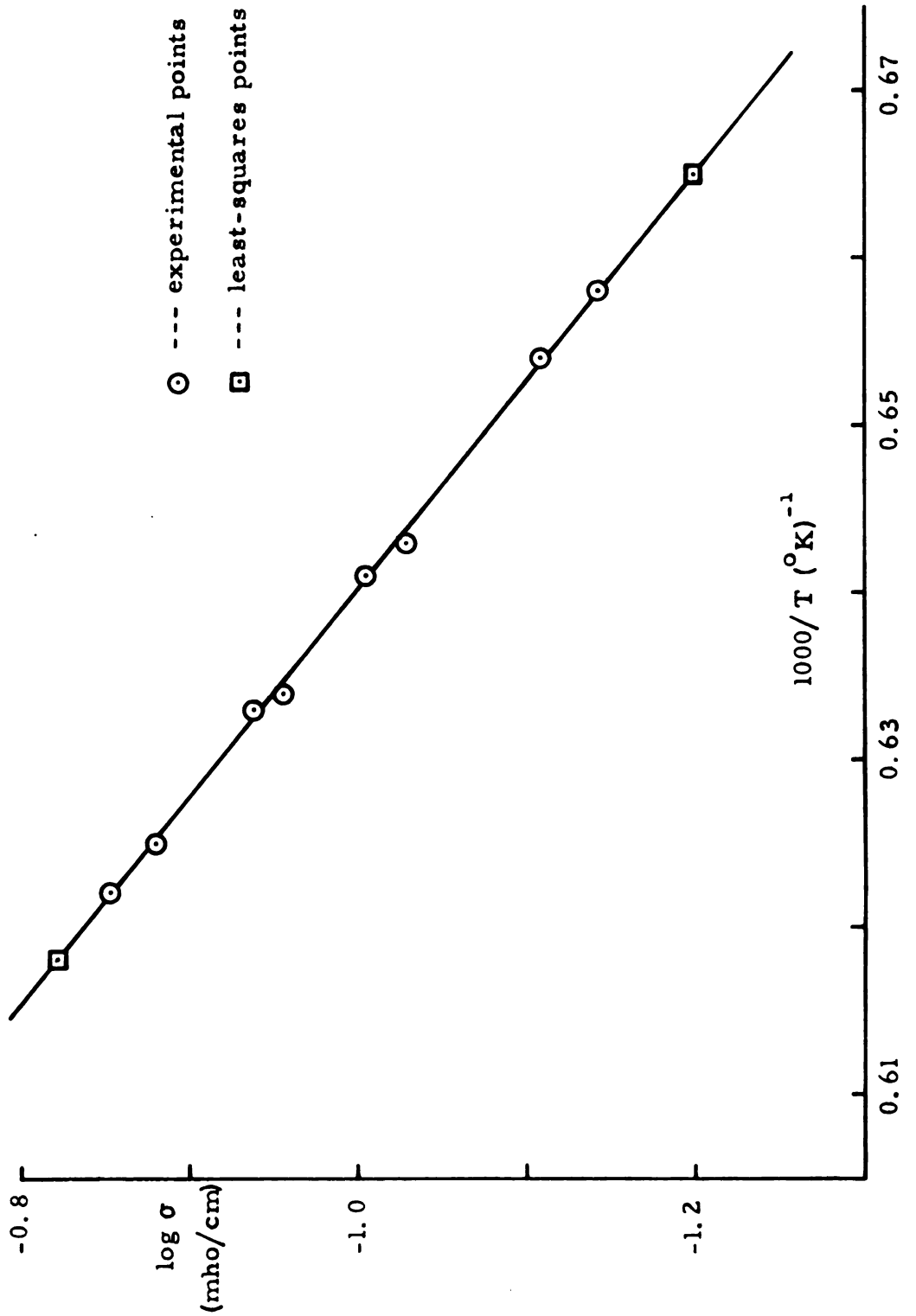

Fig. 16 - Least-squares line for sample 4SC(c)

V. DISCUSSION

The experimental results clearly show that the electrical conductivity of pure Cr_2O_3 exhibits intrinsic behavior above a characteristic temperature which varies from one sample to another, and is dependent upon oxygen pressure below that temperature. For the unoriented samples this characteristic temperature is approximately 1100°C, and for the oriented samples it is approximately 1250°C. Figures 10 and 13 show this effect for samples 3SC and 4SC(a).

The conductivity in the defect-controlled region (low temperatures) is apparently quite complicated. The possible sources of conductivity in this region are (1) the defect structure of the host crystal, (2) impurities, (3) an intrinsic reaction and (4) ionic conductivity. The first and fourth mechanisms mentioned will be dependent upon oxygen pressure whereas the third will not. The contribution from impurities may also vary with oxygen pressure if the predominant impurities can easily change their valence state with change in oxygen pressure. Hence the pressure dependence could be a complicated function of several mechanisms.

The contribution from the ionic conductivity will be several orders of magnitude below the total conductivity[13] at all temperatures of interest here, and will not be considered further. Since the intrinsic contribution will be small in the defect-controlled region there remains only the impurities and the host defects. The effect of impurity concentration can be seen in the different temperatures at which the oriented and unoriented samples become intrinsic. Table I shows that the predominant

impurity in the unoriented samples was aluminum, which has been shown[17] to go into Cr_2O_3 substitutionally as Al^{3+} ions on normal Cr^{3+} sites and since it has a closed-shell configuration it should not contribute to the conductivity. On the other hand the oriented samples contained relatively large amounts of both aluminum and vanadium. Since vanadium forms a V_2O_3 compound with the corundum structure it may also go into Cr_2O_3 substitutionally as a V^{3+} ion. The V^{3+} ion differs from the Al^{3+} ion, however, in its ability to change valence readily. Thus the vanadium may be the source of the higher conductivity of the oriented samples in the defect-controlled region.

The oxygen-pressure dependence of the oriented and unoriented samples would probably be different because of the variable-valence impurity present in the former. However, it is not practical to determine the pressure dependence using single-crystal samples. Figure 10 shows the results of an attempt to determine the pressure dependence of the conductivity for sample 3SC. The lack of reproducibility is due to the very long equilibration time necessary for single crystals. A rough calculation based on Hagel's[13] diffusivity values at 1300°C gives an equilibrium time of the order of 10^4 hours. It is obvious that the samples were not reaching equilibrium with the surrounding gas in the defect-controlled region. The conductivity of the oriented samples was observed to change slowly with time at constant temperature and pressure, at temperatures just below the intrinsic region. This effect can be seen in Figures 13 and 15. The conductivity of the unoriented samples under

the same circumstances showed no drift since the approach to equilibrium had become extremely slow at 1100°C.

It is obvious from the foregoing discussion that very little significant information can be obtained from the conductivity of single crystals of Cr_2O_3 in the defect-controlled region. For this reason the measurements were not extended to lower temperatures. On the other hand the conductivity in the intrinsic region does not depend on equilibration with the atmosphere or on impurity content, but should be interpretable in terms of one predominant mechanism.

Figures 10, 11, and 13 show the electrical conductivity of samples 3SC, 2SC, and 4SC(a) respectively over a combined temperature range of 569 to 1416°C with oxygen pressure as a parameter. The lack of pressure dependence in the intrinsic region was well enough established with these samples that sample 4SC(c) was studied at only one pressure, as shown in Figure 15. Prior to any measurements it was found necessary to "pre-condition" the samples for roughly two hours at about 1200°C. As previously mentioned, the samples did not come to equilibrium with the surrounding gas phase, but a certain amount of change was observed for a short time in the intrinsic region. This change is attributed to a slight loosening of the painted platinum electrodes at their edges. After this initial pre-conditioning period the data in the intrinsic region were quite reproducible if the measurements were restricted to temperatures below about 1400°C. Above 1400°C the measured conductivity was observed to

drift steadily to lower values at a rate dependent upon the temperature. this phenomenon was found to be due to volatilization of the sample at these temperatures with a consequent decrease in the electrode area. Restricting the experimental measurements to temperatures below 1400°C made this effect negligible in all samples except 4SC(c), which appeared to lose its electrode surface more readily than the others. Since all of the samples were prepared and pre-conditioned in the same way, the most likely explanation for this appears to be preferential thermal etching of the surface.

Figures 12, 14, and 16 show the electrical conductivity in the intrinsic region for samples 2SC, 4SC(a), and 4SC(c) respectively along with a plot of the least-squares line obtained for each sample. Table VII is a tabulation of the results of the analysis for U and σ_o for these samples.

Table VII - Activation energy and pre-exponential for samples 2SC, 4SC(a), and 4SC(c) in the intrinsic region.

Sample	U (ev)	σ_o (mho/cm)
4SC(a)	1.68 ± 0.01	(1.96 ± 0.16) x 10^4
2SC	1.63 ± 0.01	(1.48 ± 0.10) x 10^4
4SC(c)	1.59 ± 0.02	(1.37 ± 0.15) x 10^4

The deviations quoted are the probable errors calculated from the scatter of points about the least-squares lines. The electrode problem previously mentioned is presumably responsible for the increased scatter of points

and consequent larger uncertainty in the activation energy for sample 4SC(c).

Figure 17 shows the intrinsic lines for all three samples. Because the electrode geometry was known to change slightly, the relative positions of the three lines probably are not very significant. Although the data used in the analyses were quite reproducible, the apparent anisotropy in the activation energy is so small that very little significance can be attached to it. It is difficult to estimate from the complicated crystal structure just what effect the crystalline anisotropy would have on a given conduction mechanism.

The interpretation of the experimental conductivity data would be considerably easier if some information concerning mobility were available. Unfortunately it is not experimentally possible at present to determine the mobility for transition metal oxides at high temperatures with any reliability. However, some limits on the mobility can be deduced from simple arguments. From the observed variation in magnitude of the extrinsic conductivity attributed to impurities, a lower limit for the concentration of charge carriers is estimated to be approximately 5×10^{-17} cm^{-3}. This corresponds to about ten parts per million which is roughly equivalent to the smallest impurity concentrations observed. At the other extreme the carrier concentration is certainly no greater than 5×10^{22} cm^{-3}, which is approximately the number of cations in the lattice. From equation (III-6) and the experimental results for the

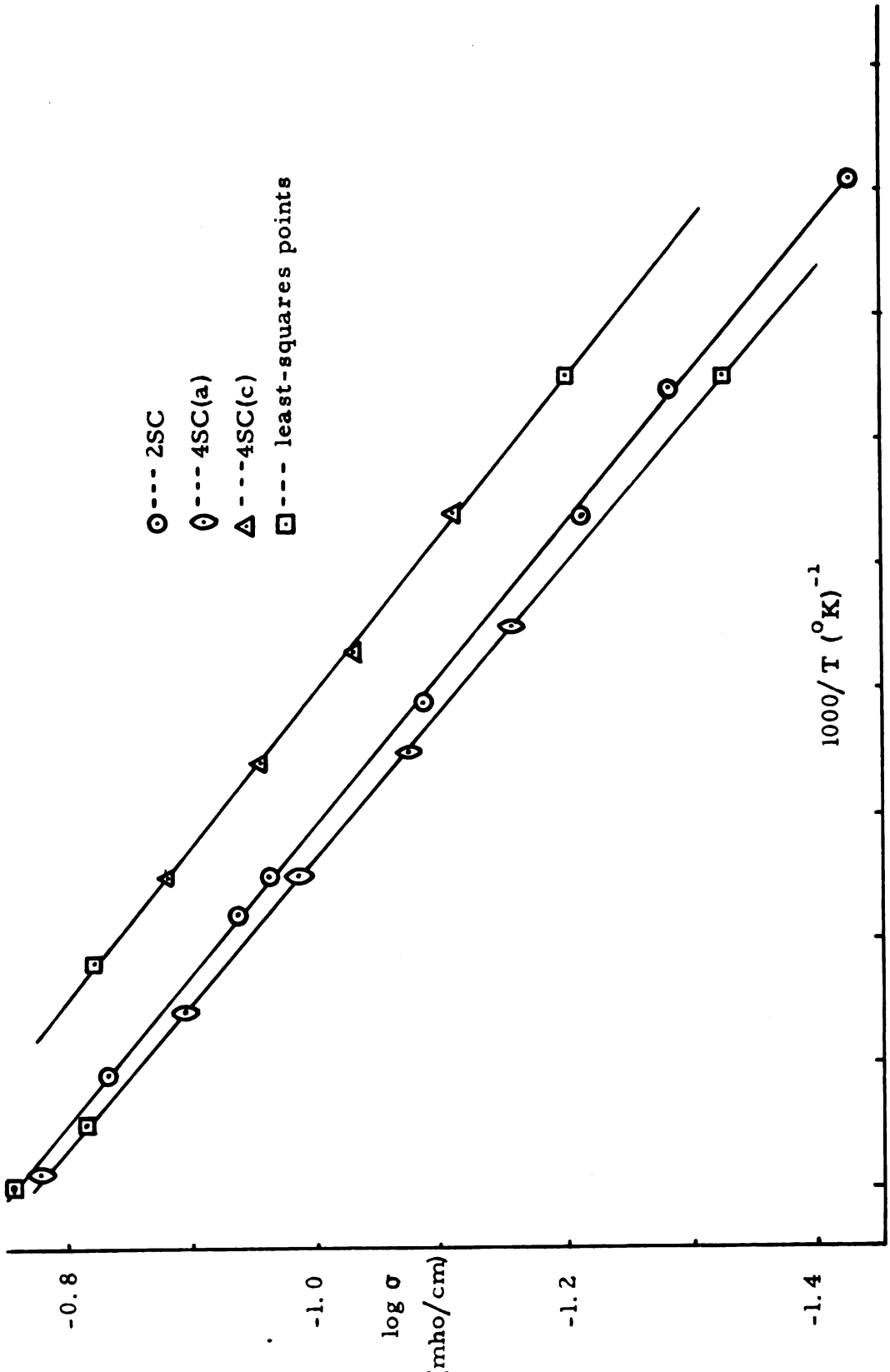

Fig. 17 - Intrinsic conductivity of samples 2SC, 4SC(a), and 4SC(c)

conductivity at 1200°C, the corresponding mobility range would be 1 to 10^{-5} cm^2/volt-sec at that temperature. This range of low mobilities is indicative either of conduction in a very narrow band or of charge transport by hopping of the carriers between localized sites. In either case, of the four intrinsic equations suggested the relevant mechanism is probably

$$2\,Cr^{3+} \rightarrow Cr^{2+} + Cr^{4+}. \qquad \text{(III-4)}$$

The distinction between a very narrow d band and hopping transport cannot be made without further experimental evidence, if it can be made at all. The possibility exists of a continuous transition from very narrow bands to isolated states with a small change of lattice spacing. It is not at all clear how this situation could be studied experimentally.

The intrinsic mechanisms described in equations (III-2) and (III-3) cannot be ruled out completely, but they seem less likely since the conductivity would be dominated by the band component which would have a high mobility. Morin[5] calculated a mobility of the order of 100 cm^2/volt-sec for NiO on the basis of conductivity by 2p holes in the valence band. This process would completely dominate any contribution from electrons in the 3d levels. A similar argument holds for electrons in the 4s band and holes in the 3d levels. The possibility of band-to-band transitions as described by equation (III-1) can probably be ruled out by the large energies observed optically for the absorption edges of the metal oxides.

VI. CONCLUSIONS

Measurements of the electrical conductivity of single crystal Cr_2O_3 as a function of temperature and oxygen partial pressure have clearly shown that there is a dependence of the conductivity on oxygen pressure below a characteristic temperature which appears to depend upon the impurity content of the material. The functional dependence of the conductivity on oxygen pressure probably depends upon the type and concentration of impurity as well as the properties of the host crystal, but this cannot be determined from measurements on single crystals owing to the excessive equilibrium time involved.

The conductivity measurements have also shown that there is an "intrinsic" type of charge transport at high temperatures which is independent of oxygen pressure. Because of the low mobility deduced from the measurements, the usual band theory of semiconductors does not seem as appropriate to use for interpretation as does the theory of small polarons. The experimental results are best interpreted in terms of charge transport on the cation lattice, which is just the model for which the theory of small polarons was devised. Although the evidence is not conclusive in itself, it is strongly in favor of the interpretation suggested. Some means of separating the charge concentration and the mobility is needed to complete the argument.

Bibilography

1. E.J.W. Verwey, Semiconducting Materials, p. 151, Butterworths, London (1951).

2. R. R. Heikes and W. D. Johnston, "Mechanism of Conduction in Li-Substituted Transition Metal Oxides," J. Chem. Phys. 26, 582 (1957).

3. S. van Houten, "Semiconduction in $Li_xNi_{(1-x)}O$," J. Phys. Chem. Solids 17, 7 (1960).

4. F. J. Morin, "Electrical Properties of α Fe_2O_3 and α Fe_2O_3 Containing Titanium," Phys. Rev. 83, 1005 (1951); "Electrical Properties of αFe_2O_3," Phys. Rev. 93, 1195 (1954); "Electrical Properties of NiO," Phys. Rev. 93, 1199 (1954).

5. F. J. Morin, "Oxides of the 3d Transition Metals," Bell System Tech. J. 37, 1047 (1958).

6. F. J. Morin, "Oxides Which Show a Metal-to-Insulator Transition at the Néel Temperature," Phys. Rev. Letters 3, 34 (1959).

7. T. D. Schultz, "Slow Electrons in Polar Crystals: Self-Energy, Mass, and Mobility," Phys. Rev. 116, 526 (1959).

8. J. Yamashita and T. Kurosawa, "On Electronic Current in NiO," J. Phys. Chem. Solids 5, 34 (1958).

9. G. L. Sewell, "Electrons in Polar Crystals," Phil. Mag. 36, 1361 (1958).

10. T. Holstein, "Studies of Polaron Motion Part I. The Molecular-Crystal Model," Ann. Phys. 8, 325 (1959); "Studies of Polaron Motion Part II. The 'Small' Polaron," Ann. Phys. 8, 343 (1959).

11. K. Hauffe and J. Block, "Fehlordnungsmodell eines Eigenstörstellen-Halbleiters am Beispiel des Chromoxyds," Z. Physik. Chem. 198, 232 (1951).

12. W. A Fischer and G. Lorenz, "Die Sauerstoffdruckabhängigkeit der elecktrischen Eigenschaften des Chrom(III)oxydes," Z. Physik. Chem. NF, 18, 308 (1958).

13. W. C. Hagel and A. U. Seybolt, "Cation Diffusion in Cr_2O_3," J. Electrochem. Soc. 108, 1146 (1961).

14. Linde Co., Crystal Products Dept., 4120 Kennedy Ave., East Chicago, Indiana.

15. Engelhard Ind., Hanovia Liquid Gold Div., 113 Astor St., Newark 2, N. J.

16. B. E. Walker et al, "Thermoelectric Instability of Some Noble Metal Thermocouples at High Temperatures," Rev. Sci. Inst. 33, 1029 (1962).

17. J. Graham, "Lattice Spacings and Colour in the System Alumina-Chromic Oxide," J. Phys. Chem. Solids 17, 18 (1960).

18. R.W.G. Wyckoff, Crystal Structures, Vol. I, Interscience Publishers, New York and London, (1948).

19. B. N. Brockhouse, "Antiferromagnetic Structure in Cr_2O_3," J. Chem. Phys. 21, 961 (1953).

20. F. A. Kröger and H. J. Vink, "Relations between the Concentrations of Imperfections in Crystalline Solids," Solid State Physics Vol. 3, 307, Academic Press, New York,(1956).

21. L. C. Walters and R. E. Grace, "Self-Diffusion of Chromium in Single Crystals of Cr_2O_3," J. Electrochem. Soc. 110, 192C, Abstract No. 194 (1963).

22. C. Kittel, Introduction to Solid State Physics, p. 352, 2nd Edition, Wiley, New York, (1956).

23. H. Margenau and G. M. Murphy, The Mathematics of Physics and Chemistry, p. 519, Van Nostrand, New York, (1956).